Efficient representation of topologically ordered states with restricted Boltzmann machines

Sirui Lu,[1,2] Xun Gao,[2,3,*] and L.-M. Duan[2,†]
[1]*Department of Physics, Tsinghua University, Beijing 100084, China*
[2]*Center for Quantum Information, Institute for Interdisciplinary Information Sciences, Tsinghua University, Beijing 100084, China*
[3]*Department of Physics, Harvard University, Cambridge, Massachusetts 02138, USA*

(Received 31 October 2018; revised manuscript received 21 March 2019; published 19 April 2019)

Representation by neural networks, in particular by restricted Boltzmann machines (RBMs), has provided a powerful computational tool to solve quantum many-body problems. An important open question is how to characterize which class of quantum states can be efficiently represented with RBMs. Here, we show that RBMs can efficiently represent a wide class of many-body entangled states with rich exotic topological orders. This includes (1) ground states of double semion and twisted quantum double models with intrinsic topological orders, (2) states of the AKLT model and two-dimensional CZX model with symmetry protected topological orders, (3) states of stabilizer Fracton models with fracton topological order, and (4) (generalized) stabilizer states and hypergraph states that are important for quantum information protocols. One twisted quantum double model state considered here harbors non-Abelian anyon excitations. Our result shows that it is possible to study a variety of quantum models with exotic topological orders and rich physics using the RBM computational toolbox.

DOI: 10.1103/PhysRevB.99.155136

I. INTRODUCTION

Deep learning has become a powerful tool with wide applications [1,2]. Recently, deep learning methods have attracted considerable attention in quantum physics [3,4], especially for attacking quantum many-body problems. The difficulty of quantum many-body problems mainly originates from the exponential growth of the Hilbert space dimension. To overcome this exponential difficulty, researchers traditionally use tensor network methods [5–7] and quantum Monte Carlo (QMC) simulation [8]. However, QMC methods suffer from the sign problem [9]; tensor network methods have difficulty dealing with high dimensional systems [10] or systems with massive entanglement [11]. These issues call for new methods.

Being one of the fundamental building blocks of deep learning, the neural network has been recently employed as a compact representation of quantum many-body states [12–22]. Many variants of neural networks have been investigated numerically or theoretically, such as the restricted Boltzmann machines (RBM) [12,13,15,21], the deep Boltzmann machine (DBM) [15,16,22], and the feedforward neural network (FNN) [18]. The RBM ansatz has also been investigated for quantum information protocols [23–25]. We focus here on the RBM states which work efficiently during variational optimization although the representational power of this is somewhat limited. An important open issue is how to characterize the class of quantum many-body states that can be represented by the RBMs.

In past decades, the studies of topological order [26,27], which are beyond the framework of Landau's symmetry breaking paradigm [28], have attracted tremendous attention. There are several types of topological ordered states: the intrinsic topological ordered states feature unliftable ground state degeneracy through local perturbations; the symmetry protected topological (SPT) ordered states with a given symmetry cannot be smoothly deformed into each other without a phase transition if the deformation preserves the symmetry; the fracton topological ordered states harbor point excitations that are immobile in the three-dimensional space, i.e., fractons. While several studies have shown that the RBM can capture simple many-body states such as graph/cluster states [13,15] and toric/surface code states [13,15,21], no single study exists which represents other more exotic topological states in the condensed matter physics [26,27,29,30].

In this paper, we incorporate tools from quantum information to construct the RBM representations for other notable many-body states, focusing on different topologically ordered states. Many exotic condensed matter topological states can be described by powerful quantum information tools: (i) the hypergraph state formalism which generalizes the graph-state formalism; (ii) the stabilizer formalism [31] which describes most of the quantum error correction code; (iii) the XS-stabilizer formalism [32] which generalizes stabilizer formalism. These formalisms themselves are vital for quantum error correction [31], classical simulation of quantum circuits [33], and Bell's nonlocality [34–38]. We prove these states of (i)–(iii) can be represented by the RBM efficiently based on the properties of their wave functions. We also propose a unary representation to generalize the RBM state to higher spin systems.

These tools from quantum information provide recipes for constructing the RBM representation within their formalism. The stabilizer formalism describes many fracton models [39–44] such as Haah's code [39]. Concerning the intrinsic topological order, we show the RBM states can capture double semion of a string-net model [45,46] and many twisted

*gaoxungx@gmail.com
†lmduan@tsinghua.edu.cn

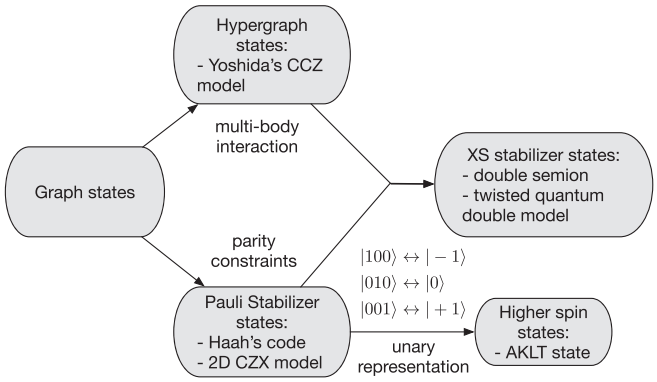

FIG. 1. Different generalizations of graph states. (a) Hypergraph states generalize graph states by introducing three-body correlation factors; (b) stabilizer states generalize graph states by additional parity constraints on qubits; (c) XS-stabilizer states combine the parity constraints from Pauli stabilizers and three-body correlation factors from hypergraph states. Many condensed matter topological models fall into these quantum information formalisms and thus can be represented efficiently by RBM. We will encounter them later. Combining with the unary representation, stabilizer states with added unary constraints can describe the AKLT state. Thus the AKLT state can be efficiently represented by the RBM.

quantum double models [47–49] using their XS-stabilizer description. For symmetry protected topological orders, we give exact constructions of the AKLT model [50,51] with the unary representation, which is thought to be impossible with RBMs [19]. We also consider RBM representation for other SPT models such as the two-dimensional (2D) CZX model [52]. Our exact representation results provide insights and a powerful tool for future studies of quantum topological phase transitions and quantum information protocols.

II. RBM STATE

We first recall the definition of the RBM state and describe notations. In the computational basis, a quantum wave function of n qubit can be expressed as $|\Psi\rangle = \sum_{\mathbf{v}} \Psi(\mathbf{v})|\mathbf{v}\rangle$ with $\mathbf{v} \equiv (v_1, \ldots, v_n)$, where the $\Psi(\mathbf{v})$ is a complex function of n binary variables v_i. We use $\{0, 1\}$ valued vertices instead of $\{-1, 1\}$ valued vertices for convenience. In the case of RBM, $\Psi(\mathbf{v}) = \sum_{\mathbf{h}} e^{W(\mathbf{v},\mathbf{h})}$, where the weight $W(\mathbf{v}, \mathbf{h}) = \sum_{i,j} W_{ij} v_i h_j + \sum_i a_i v_i + \sum_j b_j h_j$ is a complex quadratic function of binary variables. While a Boltzmann machine allows arbitrary intralayer connection, in RBM the visible neurons $\mathbf{v}$ only connect to hidden neurons $\mathbf{h}$. Let the number of visible neurons be n and the number of hidden neurons be m. We say the representation is efficient if $m = \text{poly}(n)$. The whole wave function writes

$$\Psi_{\text{RBM}}(\mathbf{v}) = e^{\sum_{i=1}^{n} a_i v_i} \prod_{j=1}^{m} [1 + \exp(\theta_j)], \tag{1}$$

with effective angles $\theta_j = b_j + \sum_{k=1}^{n} W_{kj} v_k$.

We depict this paper's roadmap in Fig. 1. RBM states [53] have been shown to represent graph states efficiently [13,15] [recall the wave function of graph states takes the form $\Psi(v_1, \ldots, v_n) = \prod_{\{i,j\}} (-1)^{v_i v_j}$ (up to a normalization factor), where $\{i, j\}$ denotes an edge linking the ith and jth qubits represented by visible neurons v_i, v_j]. There are various ways to generalize graph states. Hypergraph states [54] generalize graph states by introducing more than two body correlation factors such as $(-1)^{v_1 v_2 v_3}$. Stabilizer states generalize graph states through additional local Clifford operations [55–57], which impose parity constraints and extra phases. XS-stabilizer states [32] combine three-body correlation factors from hypergraph states and parity constraints from stabilizer states. A parity constraint, $(v_1 + v_2 + \cdots + v_k) \mod 2 = 0$, can be realized by a hidden neuron that connects to each of these visible neurons $v_1, v_2, \ldots, v_k$ with weight function $W(v, h) = i\pi vh - (\ln 2)/4$ [58]. Next we derive the RBM representation of multibody correlation factors (hypergraph states) and the unary representation, so that all the states in Fig. 1 can be represented by the RBM.

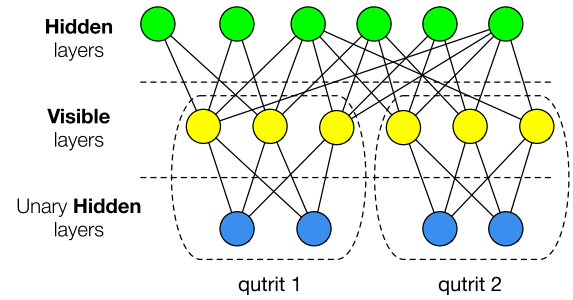

FIG. 2. Unary RBM representation for higher spin systems. The three left yellow neurons correspond to the qubit 1 and the three right yellow neurons correspond to the qubit 2. Two blue neurons in the unary hidden layers restrict three visible yellow neurons to be one of 100, 010, and 001 that correspond to $|-1\rangle$, $|0\rangle$, and $|+1\rangle$ in spin 1. The whole graph is still a bipartite graph.

III. UNARY RBM REPRESENTATION

To study higher spin systems, we propose a unary representation. The idea of unary representation is best illustrated using an example, as depicted in Fig. 2. We use three neurons (qubits) to represent a spin-1, $|100\rangle \to |-1\rangle$, $|010\rangle \to |0\rangle$, and $|001\rangle \to |1\rangle$, by restricting these three neurons (qubits) to the subspace spanned by $|100\rangle$, $|010\rangle$, and $|001\rangle$. This can be done by using two hidden neurons (blue neurons in Fig. 2) (see Appendix B for more details). Our unary representation is simpler than multivalued neurons or encoded binary neurons in distinguishing and decoding basis states. We emphasize that our unary RBMs are more powerful than RBMs with multivalue neurons; an example is that the state of the AKLT model can be represented by short-ranged unary RBMs but cannot be represented by short-ranged RBMS with ternary visible units. We will describe this example in Sec. V C.

IV. RBM REPRESENTATION OF STATES FROM QUANTUM INFORMATION FORMALISMS

A. RBM representation of hypergraph states

Hypergraphs generalize graphs by allowing an edge to join any number of vertices. We define an edge that connects k

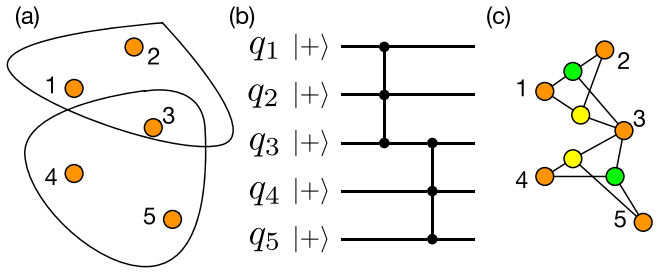

FIG. 3. RBM representation of hypergraph state. (a) A hypergraph. There are two three hyperedges that connect q_1, q_2, q_3 and q_3, q_4, q_5. (b) The encoding circuit of this hypergraph state, where $|+\rangle = (|0\rangle + |1\rangle)/\sqrt{2}$ represents the input state for all the qubits and the connected dots denote the controlled-controlled-Z gate. (c) The corresponding RBM representation of (a). Orange neurons are visible neurons, and both green and yellow vertices are hidden neurons. The two different colors (yellow and green) represent different weight functions.

vertices a k hyperedge. Given a mathematical hypergraph, the wave function of its corresponding hypergraph state [54] takes the form $\Psi_{\text{hypergraph}}(\mathbf{v}) \propto \prod_{\{v_1,v_2,\ldots,v_k\}\in E}(-1)^{v_1 v_2 \cdots v_k}$. The notation $\{v_1, v_2, \ldots, v_k\} \in E$ means that these k vertices $\{v_1, v_2, \ldots, v_k\}$ are connected by a k hyperedge. We illustrate the correspondence in Fig. 3. We now extend RBM representation to hypergraph states.

Theorem 1. Restricted Boltzmann machines can represent any hypergraph states efficiently and exactly.

In the main text, we take the graph with three hyperedges as an example; it will be useful later for representation of XS-stabilizer states and SPT states. Precisely, we make use of the following decomposition:

$$(-1)^{v_1 v_2 v_3} = e^{i\pi(\sum_{i=1}^{3} v_i)} \sum_{h_1,h_2} e^{w(\sum_{i=1}^{3} v_i)(h_1-h_2)+b(h_1+h_2)+c}, \quad (2)$$

where $w = i$, $b = \ln(\frac{1+\sqrt{-15}}{4})$, and $c = \ln\frac{2}{3} - b$. Thus the exact RBM representation of $(-1)^{v_1 v_2 v_3}$ uses two hidden neurons, as shown in Fig. 3(c). The method for decomposing $(-1)^{v_1 v_2 v_3}$ can be extended to treat $(-1)^{v_1 v_2 \cdots v_k}$ for arbitrary k with $2k + O(1)$ hidden neurons [59].

B. RBM representation of XS/Pauli-stabilizer states

The Pauli stabilizer formalism generalizes graph states by applying some local Clifford transformations [56,60]. The XS-stabilizer formalism generalizes the Pauli stabilizer formalism [32] by changing the single qubit Pauli group to Pauli-S group $\mathcal{P}^S = \langle \alpha I, X, S\rangle$, where $\alpha = e^{i\pi/4}$ and $S = \text{diag}(1, i)$. We have the following theorem based on the key observation that the wave function of the stabilizer state (proved in [55,61–63]) and the similar result on the XS-stabilizer state (proved in [32]).

Theorem 2. Restricted Boltzmann machines can represent any Pauli-stabilizer states and XS-stabilizer states efficiently and exactly.

Let $\delta(x)$ be a Boolean function which satisfies $\delta(0) = 1$ and $\delta(1) = 0$. The wave functions of every Pauli-stabilizer state and XS-stabilizer state on n qubits can be written as the closed form of

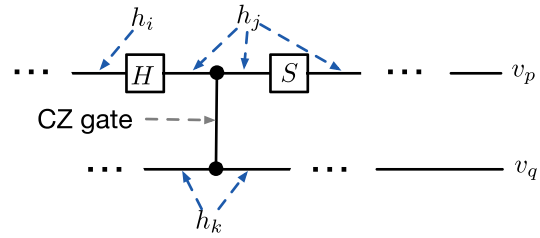

FIG. 4. Closeup of a Clifford circuit. Visible neurons are $v_p, v_q, \ldots$ and hidden neurons are $h_i, h_j, \ldots$. Each H gate corresponds to two neurons with the weight $(-1)^{x_i x_j}$. Each S gate corresponds to one neuron with the weight i^{x_j}; each CZ gate corresponds to two neurons with the weight $(-1)^{x_1 x_2}$. The whole wave function is a DBM which can be eliminated to a RBM.

$$\Psi_{\text{Pauli}}(\mathbf{v}) \propto i^{l(\mathbf{v})}(-1)^{q(\mathbf{v})} \prod_j \delta\big(L_j^p \bmod 2\big), \quad (3)$$

$$\Psi_{\text{XS}}(\mathbf{v}) \propto \alpha^{l(\mathbf{v})} i^{q(\mathbf{v})}(-1)^{c(\mathbf{v})} \prod_j \delta\big(L_j^p \bmod 2\big), \quad (4)$$

where $l(\mathbf{v})$, $q(\mathbf{v})$, and $c(\mathbf{v})$ are linear, quadratic, and cubic polynomials of $\mathbf{v}$ with integer coefficients, respectively. The L_j^p are affine (linear terms plus constant term) functions of some subsets of $\mathbf{v}$. Moreover, the polynomials $l(x)$, $q(x)$, and $c(x)$ along with L_j^p can be determined efficiently from the given stabilizers.

Given this wave function, we can easily deduce its RBM representation. First, the $\prod_j \delta(L_j^p \bmod 2)$ parts correspond to parity constraints, which RBM can represent. Meanwhile, functions that are products of $i^{l(\mathbf{v})}$, $(-1)^{q(\mathbf{v})}$, $\alpha^{l(\mathbf{v})}$, $i^{q(\mathbf{v})}$, and $(-1)^{c(\mathbf{v})}$ can also be represented by RBM using techniques used for graph states and hypergraph states.

In the case of stabilizer states, we provide a new proof of the closed form wave function as follows. First, a stabilizer state can be generated from a Clifford circuit [31] consisting of H, S, and CZ gates. From the encoding circuit, the stabilizer state can be represented by a DBM in the closed form Eq. (3) directly. Then we can iteratively reduce it to an RBM while still keeping the closed form. The reader who is not interested in the derivation can safely skip the following detailed recipe for proving Eq. (3).

The wave function can be represented by a DBM as follows. We denote visible neurons as $v_p, v_q, \ldots$ and hidden neurons as $h_i, h_j, h_k, \ldots$. For convenience. we unify the notation of these neurons as $x_i, x_j, x_k, \ldots$ here. As shown in Fig. 4, each H gate corresponds to two neurons with the weight $(-1)^{x_i x_j}$; each S gates corresponds to one neuron with the weight i^{x_j} (even though each single qubit matrix has two indices); each CZ gate corresponds to two neurons with the weight $(-1)^{x_1 x_2}$. Multiplying together and summing over all the hidden indices, we can get the wave function of the stabilizer state:

$$\Psi(v_p, v_q, \ldots) \propto \sum_{h_i,h_j,\ldots} i^{L(h_i,h_j,\ldots,v_p,v_q,\ldots)}(-1)^{Q(h_i,h_j,\ldots,v_p,v_q,\ldots)}, \quad (5)$$

where L and Q are affine (with linear and constant terms) and quadratic (without linear term) polynomials with integer coefficients.

Next, we reduce this DBM to a RBM with the following strategy: after eliminating an h_i for some i, the remaining term still keeps the form shown in Eq. (5) except for an additional parity constraint on some of v_p, v_q, ... Here, we consider the effect of eliminating h_i in detail.

(1) If the coefficient of h_i in L is zero or 2, ignoring the terms not depending on h_i, the remaining in Eq. (5) could be written as

$$\sum_{h_i}(-1)^{h_i L_i'} = 2\delta\big(L_i^p \mod 2\big),$$

where δ means constraint and L_i^p is an affine polynomial involving those x_j which interact with h_i in Q and constant terms which are the coefficients of h_i in L. There are two cases for L_i^p.

(1.1) If L_i^p only involves visible neurons, we can put this constraint δ before the summation in Eq. (5).

(1.2) If L_i^p involves hidden neurons, e.g., h_j, then we can solve the equation $L_i^p = 0 \mod 2$ by $h_j = L_i^{p'} \mod 2$. After the summation of h_j, the only remaining terms are those satisfying $h_j = L_i^{p'} \mod 2$ so we can replace h_j by $L_i^{p'}$ in Q and by $(L^{p'})^2$ in L [because $L^{p'} \mod 2 = (L^{p'})^2 \mod 4$] in Eq. (5). The key point is the coefficients of quadratic terms in $(L^{p'})^2$ are always 2; thus they keep the same form as the terms in the summation of Eq. (5) after summation over h_i and h_j.

(2) If the coefficient of h_i in L is 1 (the case for 3 is similar), ignoring the terms not depending on h_i, the remaining in Eq. (5) can be written as

$$\sum_{h_i}(-1)^{h_i L_i^p} i^{h_i} = (1+i)i^{3(L_i^p)^2}.$$

The key point is that the coefficient of quadratic terms in $(L_i^p)^2$ is 2; thus it keeps the same form as the terms in the summation of Eq. (5) after summation over h_i.

After eliminating all the hidden variables, the wave function could be written as the form of Eq. (3).

One can make use of local Clifford equivalence between stabilizer state and graph states [56,64] to further simplify our procedure. The encoding circuit can be chosen based on the fact that every stabilizer state can be chosen to be locally equivalent to a graph state such that only at most a single H or S gate is acting on each qubit [64]. Then, the number of hidden neurons used to represent hidden variables is fewer than the number of H acting on each qubit. In total, the number of hidden neurons needed is of order $O(N_e + n)$. The N_e is the number of edges in the corresponding graph, and is at most $O(n^2)$; however, we do not usually encounter graph states from dense graphs [65], typically only $O(n \log n)$ or even $O(n)$ hidden neurons are needed. Our representation method is effective and optimal.

Next, we describe topological states with different topological orders within our quantum information framework. These topological states can be represented as RBM efficiently.

V. RBM REPRESENTATION OF TOPOLOGICALLY ORDERED STATES

A. Fracton topological order

The Pauli stabilizer formalism covers most of the fracton topological order models [39–41,44], such as Haah's code [39], X-cube model [43], and checkboard model [43]. For example, stabilizers of Haah's code involve two types of stabilizers on eight spins: eight Z operators and eight X operators in each cube. The RBM representations for states of these models can be easily deduced using our method in Sec. IV B.

B. Intrinsic topological order

We now consider RBM representation for some notable XS stabilizer states: the double semion (an example of the string-net model [45]) and many twist quantum double models. We define the double semion model on a honeycomb lattice with one qubit per edge. The wave function of double semion is $|\psi\rangle = \sum_{x \text{ is loops}}(-1)^{\text{number of loops}}|x\rangle$. In the XS-stabilizer formalism, this model has two types of stabilizer operators [32]: $g_p = \prod_{l\in v} Z_l$, $g_p = \prod_{l\in p} X_l \prod_{r\in \text{legs of } p} S_r$ corresponding to the vertex s and the face p, respectively.

Quantum double models [47] are generalizations of the toric code that describe systems of Abelian and non-Abelian anyons. Twisted quantum double models further generalize quantum double models [47–49,66,67] and are Hamiltonian realizations of Dijkgraaf-Witten topological Chern-Simons theories [68]. Many twisted quantum double models fit into the XS-stabilizer formalism [32] and thus can be represented as RBM exactly. Examples include twisted quantum double model $D^{\omega}(\mathbb{Z}_2^n)$ with the group $\mathbb{Z}_2^n$ and different twists $\omega \in H^3(\mathbb{Z}^n, U(1))$ on a triangular lattice, where $H^3(\mathbb{Z}_2^n, U(1))$ is the third cohomology group. The $H^3(\mathbb{Z}_2^1, U(1))$ case includes the double semion. It is known [32,69] that a nontrivial twist from $H^3(\mathbb{Z}_2^3, U(1))$ harbors non-Abelian anyon excitations.

C. Symmetry protected topological order

The AKLT model [50,51] is a one-dimensional spin-1 model with symmetric protected topological order. When imposing the periodic boundary condition, the unique ground state $|\psi_{AKLT}\rangle$, in terms of the matrix product state, is written

$$\Psi_{AKLT}(a_1, a_2, \ldots, a_n) \propto \mathrm{Tr}\big(A_{a_1}A_{a_2}\ldots A_{a_n}\big), \tag{6}$$

where $A_{-1} = X$, $A_0 = Y$, $A_{+1} = Z$, and $a_i = -1, 0, +1$. Alternatively, matrix product states can be described as projected entangled pair states (PEPS) [26]. As shown in Fig. 5, every red line is a EPR pair $|00\rangle + |11\rangle$. Each shaded circle represents a projection from two spins of dimension 2 to a physical degree of dimension 3 (spin-1). $P = \sum_{a_i,\alpha,\beta} A_{a_i,\alpha,\beta}|a_i\rangle\langle\alpha\beta|$, where the summation is over $a_i = -1, 0, 1$ and $\alpha, \beta = 1, 2$. After using unary representation, in the quantum circuit language, the projection P is a map that maps $|01\rangle + |10\rangle \to |100\rangle$, $i(|01\rangle - |10\rangle) \to |010\rangle$, and $|00\rangle - |11\rangle \to |001\rangle$. We find such a quantum circuit made of Clifford gate, as shown in Fig. 5(b). Because all operations are Clifford gates, the whole quantum state is a Pauli stabilizer state restricted to the single excitation subspace spanned by $|001\rangle$, $|010\rangle$, and $|100\rangle$. Thus

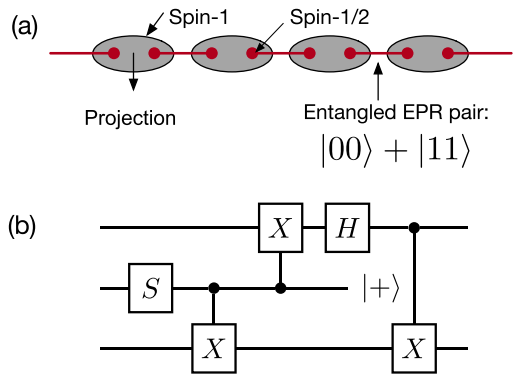

FIG. 5. (a) Ground state of the AKLT model. The spin one on each lattice site can be decomposed into two spin 1/2's which form EPR pairs between nearest neighbor pairs. At the two ends of an open chain, there are two isolated spin 1/2's giving rise to a fourfold ground state degeneracy. Every red line represents a $|00\rangle + |11\rangle$ state. Each shaded circle represents a projection operator $P = |100\rangle(\langle 01| + \langle 10|) + |010\rangle i(\langle 01| - \langle 10|) + |001\rangle(\langle 00| - \langle 11|)$. (b) The Clifford circuit that realizes the projection P under the unary representation (living in the space spanned by $|100\rangle$, $|010\rangle$ and $|001\rangle$). Here $|+\rangle$ means projecting onto the $|+\rangle$ state.

it can be represented by RBM with unary hidden neurons (blue neurons in Fig. 2) and other hidden neurons [70].

We also show RBM can represent other symmetry-protected topologically ordered states. These examples include the 2D CZX model (with $\mathbb{Z}_2$ symmetry), and Yoshida's CCZ model [71] (with $\mathbb{Z}_2 \otimes \mathbb{Z}_2 \otimes \mathbb{Z}_2$ symmetry). The ground state of the 2D CZX model [52] is a tensor product of GHZ states $|0000\rangle + |1111\rangle$ on each plaquette. Because the GHZ states belong to stabilizer states, RBM can exactly represent the ground state of the 2D CZX model. Similar to SPT cluster states, the ground state of Yoshida's CCZ model [40] on the trivalent lattice is a hypergraph state with three hyperedges. Thus it can also be represented efficiently by RBMs.

VI. CONCLUSION AND DISCUSSION

This paper sets out to investigate different topological models with RBM representation using tools from quantum information such as the (XS) stabilizer and the (hyper) graph-state formalisms. The most significant findings are the fact that RBM states can capture ground states of exotic models with different types of topological orders, including intrinsic topological orders, symmetry protected topological orders, and fracton topological orders. It remains open whether RBM can capture additional string-net models with more exotic non-Abelian anyon excitations such as the states of the double Fibonacci model [45]. The RBM state may be helpful in investigating symmetry enriched topological order [72] and symmetry fractionalization [73]. We remark that our method also generalizes conveniently to qudit stabilizer states [64] with the proposed unary representation. Our exact representation results provide useful guidance for future numerical studies on topological phase transitions.

Our results are also of interest from the quantum information perspective. The Gottesman-Knill theorem [33,65,74] states that stabilizer dynamics can be efficiently simulated. Our result which shows RBM states contain stabilizer states suggests classical simulation of an unknown larger family of quantum circuits may benefit from the RBM representation [24]. Because hypergraph states allow for an exponentially increasing violation of the Bell inequalities [34–37], our results provide analytical evidence for numerical studies [13] on estimating maximum violation of Bell inequalities.

Note added. Recently, a report appeared [75] which gives a different method to represent stabilizer states with the restricted Boltzmann machine.

ACKNOWLEDGMENTS

We thank Giuseppe Carleo, Dong-Ling Deng, Sheng-Tao Wang, Mingji Xia, Shunyu Yao, Fan Ye, Zhengyu Zhang, and You Zhou for helpful discussions. This work was supported by Tsinghua University and the National Key Research and Development Program of China (Grant No. 2016YFA0301902).

APPENDIX A: DETAILED DERIVATION OF RBM REPRESENTATIONS OF HYPERGRAPH STATES

First we recall the definition of the quantum hypergraph state in more detail. Mathematically, hypergraphs are generalizations of graphs in which an edge may connect more than two vertices. Formally, a hypergraph H is a pair $H = (X, E)$ where X is a set of elements called vertices and E is a subset of $P(X)$, where $P(X)$ is the power set of X. Given a mathematical hypergraph, the corresponding quantum state can be generated by following similar steps in constructing a graph state: first, assign to each vertex a qubit and initialize each qubit as $|+\rangle$; then, whenever there is hyperedge, perform a controlled-Z operation between all connected qubits; if the qubits $v_1, v_2, \ldots, v_k$ are connected by a k hyperedge, then perform $C^k Z_{i_1,i_2,\ldots,i_k}$. As a result, the hypergraph state and its wave function [54] take the form

$$|g\rangle = \prod_{\{i_1,i_2,\ldots,i_k\}\in E} C^k Z_{i_1,i_2,\ldots,i_k} |+\rangle^{\otimes n},$$

$$\Psi(g) = \sum_{v_1,v_2,\ldots,v_n} \prod_{\{i_1,i_2,\ldots,i_k\}\in E} (-1)^{i_1 i_2 \ldots i_k} |v_1 v_2 \cdots v_n\rangle. \quad \text{(A1)}$$

Next, we give a detailed derivation of realizing the correlation factor of the type $(-1)^{v_1 v_2 \cdots v_k}$ using restricted Boltzmann machines. We first recall $(-1)^{v_1 v_2}$ which relates to graph states from [15]:

$$H_{v_1,v_2} = \frac{(-1)^{v_1 v_2}}{\sqrt{2}} = \sum_{h=0,1} e^{W_H(v_1,h)+W_H(v_2,h)}$$

$$= \cos\left(\frac{\pi}{4}[2(v_1+v_2)-1]\right). \quad \text{(A2)}$$

Note the above equation (A2) is only true for $v_i = 0, 1$. By $\cos v = \frac{1}{2}(e^{iv} + e^{-iv}) = \sum_h e^{iv(2h-1)-\ln 2}$, we have an explicit formula for W_H:

$$W_H(v_i, h) = i\pi v_i h - i\pi[2v_i + h]/4 + (i\pi/4 - \ln 2)/2$$

$$= \frac{\pi}{8} i - \frac{\ln 2}{2} - \frac{\pi}{2} iv - \frac{\pi}{4} ih + i\pi vh.$$

Then we consider $(-1)^{v_1v_2v_3}$ with the following decomposition:

$$\begin{aligned}&(-1)^{v_1v_2v_3}\\&=(-1)^{v_1+v_2+v_3}\left[\frac{8}{3}\cos^2\left(\frac{2\pi}{3}(v_1+v_2+v_3-1)+\frac{\pi}{2}\right)-1\right]\\&=e^{i\pi(v_1+v_2+v_3)}\left[\frac{1}{3}+\frac{4}{3}\cos\left(\frac{4\pi}{3}(v_1+v_2+v_3)-\frac{\pi}{3}\right)\right].\end{aligned}$$

Let $v=\frac{4\pi}{3}(v_1+v_2+v_3)-\frac{\pi}{3}$. The above equation simplifies to

$$\begin{aligned}(-1)^{v_1v_2v_3}&=e^{i\pi(v_1+v_2+v_3)}\left(\tfrac{1}{3}+\tfrac{4}{3}\cos v\right)\\&=e^{i\pi(v_1+v_2+v_3)}\left(\tfrac{1}{3}+\tfrac{2}{3}(e^{iv}+e^{-iv})\right).\end{aligned}$$

The RBM can represent the first part by definition. We consider the second part as a RBM with two hidden neurons and set equations:

$$\begin{aligned}&\frac{1}{3}+\frac{2}{3}(e^{iv}+e^{-iv})\\&=\sum_{h_1,h_2}e^{wvh_1+w_2vh_2+b_1h_1+b_2h_2+c}\\&=e^c(1+e^{w_1v+b_1}+e^{w_2v+b_2}+e^{(w_1+w_2)v+b_1+b_2}).\end{aligned}$$

Solving the above equation, we get $w_1=-w_2=\sqrt{-1}$, $b_1=b_2=b$, and

$$e^c(1+e^{2b})=\tfrac{1}{3},\quad e^{b+c}=\tfrac{2}{3}.$$

Solving the above system of equations, we obtain

$$b=\ln\left(\frac{1\pm i\sqrt{15}}{4}\right),\quad c=\ln\frac{2}{3}-b.$$

In fact, this construction can be extended to any function of the form $(-1)^{v_1v_2\cdots v_k}$. The proof goes as follows. First, we generalize our construction a bit to simulate the correlation factor $2A\cos(\sum_{i=1}^k v_i)+B$ by two hidden neurons. Setting the equation

$$\begin{aligned}&\sum_{h_1,h_2}e^{w_1(\sum_{j=1}^k v_j)h_1+w_2(\sum_{j=1}^k v_j)h_2+b_1h_1+b_2h_2}\\&\quad=A(e^{i(\sum_{i=1}^k v_j)}+e^{-i(\sum_{j=1}^k v_j)})+B.\end{aligned}$$

Simplifying the above equation, we obtain

$$w_1=-w_2=i,\quad e^{c+b_1}=e^{c+b_2}=A,\quad e^c(1+e^{b_1+b_2})=B.$$

Solving the system of equations, we get

$$\begin{aligned}b=b_1=b_2&=\ln\left(\frac{B\pm\sqrt{B^2-4A^2}}{2A}\right),\\c=\ln A-b&=\ln A=\ln\frac{2A^2}{B\pm\sqrt{B^2-4A^2}}.\end{aligned}$$

Now we proceed to construct RBM representation for $g(v_1,v_2,\ldots,v_k)=(-1)^{v_1v_2\cdots v_k}$. Note $g(v_1,v_2,\ldots,v_k)$ is equal to 1 only if $v_1=v_2=\cdots v_k=1$, i.e., $v_1+v_2+\cdots+v_k=k$. For convenience, we first consider

$$\begin{aligned}f\left(\sum_{i=1}^k v_i\right)&=\frac{1}{2}\left[1-g\left(\sum_{i=1}^k v_i\right)\right]\\&=\begin{cases}1, & v_1+v_2+\cdots v_k=k,\\0, & \text{otherwise.}\end{cases}\end{aligned}$$

The trick of the construction is to introduce the function

$$\begin{aligned}t\left(\sum_{i=1}^k v_i\right)&=\cos\left(\frac{2\pi}{k+1}(v_1+v_2+\cdots+v_k+1)\right)\\&=\begin{cases}1, & v_1+v_2+\cdots v_k=k,\\\text{other values} & \text{otherwise.}\end{cases}\end{aligned}$$

Then the function f can be chosen as (the idea is similar to Lagrange polynomial method)

$$f\left(\sum_{i=1}^k v_i\right)=\prod_{i=0}^k\frac{t\left(\sum_{i=1}^k v_i\right)-t(i)}{t(i)-t(1)}=\begin{cases}1, & \sum_{i=1}^k v_i=k,\\0, & \text{otherwise.}\end{cases}$$

Then by substitution we get g:

$$g=1-2f=1-2\prod_{i=0}^k\frac{t\left(\sum_{i=1}^k v_i\right)-t(i)}{t(i)-t(1)}.$$

In principle we can factorize g into the form of $g(t)=\prod_i(2C_it+D_i)$, which can then be simulated by RBM term by term.

Now we remark on the relation between our decomposition and Eq. (27) in [22]. These two mainly differ in the choice of the basis. We use a $\{0,1\}$ basis in contrast to the $\{-1,+1\}$ basis in [22]. This difference leads to several consequences. First, in the $\{0,1\}$ basis, $(-1)^{x_1x_2x_3}$ is only equal to -1 when all the x_i is equal to 1. While, in the $\{-1,+1\}$ basis, $e^{x_1x_2x_3V}$ is equal to e^V or e^{-V} if the number of -1 in x_i is even/odd. That's the reason why the latter decomposition only needs two hidden neurons. If we derive a similar RBM expression of our n-body gadget from Eq. (27) in [22] directly, $O(2^k)$ hidden neurons are needed. In contrast our cost is $2k+O(1)$. Meanwhile, the correlation factor of graph/hypergraph states $(-1)^{x_1x_2x_3}$ is somewhat meaningless in the $\{-1,+1\}$ basis.

APPENDIX B: DERIVATION DETAILS OF RBM UNARY REPRESENTATIONS

Restricting three neurons only take values from 100, 010, and 001 equivalently to construct the RBM representation of a W state: $|W\rangle=(|001\rangle+|010\rangle+|001\rangle)/\sqrt{3}$. This can be done by two hidden neurons as follows. Consider the function

$$h(v_1,v_2,v_3)=\begin{cases}1, & v_1+v_2+v_3=1,\\0, & \text{otherwise.}\end{cases}$$

We find a decomposition of $h(v_1,v_2,v_3)$:

$$h(v_1,v_2,v_3)=(-1)^{\sum_{i=1}^3 v_i}\left\{-\frac{1}{3}+\frac{2}{3}\cos\left[\frac{4\pi}{3}\left(\sum_{i=1}^3 v_i\right)-\frac{\pi}{3}\right]\right\},$$

which can be simulated using two hidden neurons and the method from the last section. The weights can be easily computed.

When we want to use unary neurons for spin-$k/2$ systems, we need the generalized W states $W_{n,k}$, which are defined to be a uniform superposition of all computational basis states $|x\rangle$ where x is a Hamming weight k bit string. These states can be represented by RBM using nearly the technique from Appendix A.

[1] Y. LeCun, Y. Bengio, and G. Hinton, Deep learning, Nature (London) **521**, 436 (2015).

[2] I. Goodfellow, Y. Bengio, A. Courville, and Y. Bengio, *Deep Learning* (MIT Press, Cambridge, MA, 2016), Vol. 1.

[3] J. Biamonte, P. Wittek, N. Pancotti, P. Rebentrost, N. Wiebe, and S. Lloyd, Quantum machine learning, Nature (London) **549**, 195 (2017).

[4] C. Ciliberto, M. Herbster, A. D. Ialongo, M. Pontil, A. Rocchetto, S. Severini, and L. Wossnig, Quantum machine learning: a classical perspective, Proc. R. Soc. A **474**, 20170551 (2018).

[5] U. Schollwöck, The density-matrix renormalization group in the age of matrix product states, Ann. Phys. (NY) **326**, 96 (2011).

[6] F. Verstraete, V. Murg, and J. I. Cirac, Matrix product states, projected entangled pair states, and variational renormalization group methods for quantum spin systems, Adv. Phys. **57**, 143 (2008).

[7] N. Schuch, M. M. Wolf, F. Verstraete, and J. I. Cirac, Simulation of Quantum Many-Body Systems with Strings of Operators and Monte Carlo Tensor Contractions, Phys. Rev. Lett. **100**, 040501 (2008).

[8] D. Ceperley and B. Alder, Quantum Monte Carlo, Science **231**, 555 (1986).

[9] E. Y. Loh, J. E. Gubernatis, R. T. Scalettar, S. R. White, D. J. Scalapino, and R. L. Sugar, Sign problem in the numerical simulation of many-electron systems, Phys. Rev. B **41**, 9301 (1990).

[10] N. Schuch, M. M. Wolf, F. Verstraete, and J. I. Cirac, Computational Complexity of Projected Entangled Pair States, Phys. Rev. Lett. **98**, 140506 (2007).

[11] F. Verstraete, M. M. Wolf, D. Perez-Garcia, and J. I. Cirac, Criticality, the Area Law, and the Computational Power of Projected Entangled Pair States, Phys. Rev. Lett. **96**, 220601 (2006).

[12] G. Carleo and M. Troyer, Solving the quantum many-body problem with artificial neural networks, Science **355**, 602 (2017).

[13] D.-L. Deng, X. Li, and S. Das Sarma, Machine learning topological states, Phys. Rev. B **96**, 195145 (2017).

[14] S. R. Clark, Unifying neural-network quantum states and correlator product states via tensor networks, J. Phys. A: Math. Theor. **51**, 135301 (2018).

[15] X. Gao and L.-M. Duan, Efficient representation of quantum many-body states with deep neural networks, Nat. Commun. **8**, 662 (2017).

[16] Y. Huang and J. E. Moore, Neural network representation of tensor network and chiral states, arXiv:1701.06246.

[17] D.-L. Deng, X. Li, and S. Das Sarma, Quantum Entanglement in Neural Network States, Phys. Rev. X **7**, 021021 (2017).

[18] Z. Cai and J. Liu, Approximating quantum many-body wave functions using artificial neural networks, Phys. Rev. B **97**, 035116 (2018).

[19] J. Chen, S. Cheng, H. Xie, L. Wang, and T. Xiang, Equivalence of restricted Boltzmann machines and tensor network states, Phys. Rev. B **97**, 085104 (2018).

[20] I. Glasser, N. Pancotti, M. August, I. D. Rodriguez, and J. I. Cirac, Neural-Network Quantum States, String-Bond States, and Chiral Topological States, Phys. Rev. X **8**, 011006 (2018).

[21] Z.-A. Jia, Y.-H. Zhang, Y.-C. Wu, G.-C. Guo, and G.-P. Guo, Efficient machine learning representations of surface code with boundaries, defects, domain walls and twists, Phys. Rev. A **99**, 012307 (2019).

[22] G. Carleo, Y. Nomura, and M. Imada, Constructing exact representations of quantum many-body systems with deep neural networks, Nat. Commun. **9**, 5322 (2018).

[23] G. Torlai, G. Mazzola, J. Carrasquilla, M. Troyer, R. Melko, and G. Carleo, Neural-network quantum state tomography, Nat. Phys. **14**, 447 (2018).

[24] B. Jónsson, B. Bauer, and G. Carleo, Neural-network states for the classical simulation of quantum computing, arXiv:1808.05232.

[25] D.-L. Deng, Machine Learning Detection of Bell Nonlocality in Quantum Many-Body Systems, Phys. Rev. Lett. **120**, 240402 (2018).

[26] B. Zeng, X. Chen, D.-L. Zhou, and X.-G. Wen, Quantum information meets quantum matter—from quantum entanglement to topological phase in many-body systems, arXiv:1508.02595.

[27] X.-G. Wen, *Quantum Field Theory of Many-body Systems: From the Origin of Sound to an Origin of Light and Electrons* (Oxford University Press on Demand, Oxford, 2004).

[28] L. D. Landau and E. M. Lifshitz, *Statistical Physics*, Course of Theoretical Physics Vol. 5 (Butterworth-Heinemann, 1980), Vol. 30.

[29] X. Chen, Z.-C. Gu, Z.-X. Liu, and X.-G. Wen, Symmetry-protected topological orders in interacting bosonic systems, Science **338**, 1604 (2012).

[30] C.-K. Chiu, J. C. Y. Teo, A. P. Schnyder, and S. Ryu, Classification of topological quantum matter with symmetries, Rev. Mod. Phys. **88**, 035005 (2016).

[31] D. Gottesman, Stabilizer codes and quantum error correction, Ph.D. thesis, California Institute of Technology, Pasadena, California, 2004.

[32] X. Ni, O. Buerschaper, and M. Van den Nest, A non-commuting stabilizer formalism, J. Math. Phys. **56**, 052201 (2015).

[33] D. Gottesman, The Heisenberg representation of quantum computers, arXiv:quant-ph/9807006.

[34] M. Gachechiladze, C. Budroni, and O. Guhne, Extreme Violation of Local Realism in Quantum Hypergraph States, Phys. Rev. Lett. **116**, 070401 (2016).

[35] O. Guhne, M. Cuquet, F. E. S. Steinhoff, T. Moroder, M. Rossi, D. Bruß, B. Kraus, and C. Macchiavello, Entanglement and nonclassical properties of hypergraph states, J. Phys. A: Math. Theor. **47**, 335303 (2014).

[36] J. S. Bell, On the Einstein Podolsky Rosen paradox, Phys. Phys. Fiz. **1**, 195 (1964).
[37] N. Brunner, D. Cavalcanti, S. Pironio, V. Scarani, and S. Wehner, Bell nonlocality, Rev. Mod. Phys. **86**, 419 (2014).
[38] O. Gühne, G. Tóth, P. Hyllus, and H. J. Briegel, Bell Inequalities for Graph States, Phys. Rev. Lett. **95**, 120405 (2005).
[39] J. Haah, Local stabilizer codes in three dimensions without string logical operators, Phys. Rev. A **83**, 042330 (2011).
[40] B. Yoshida, Exotic topological order in fractal spin liquids, Phys. Rev. B **88**, 125122 (2013).
[41] H. Ma, E. Lake, X. Chen, and M. Hermele, Fracton topological order via coupled layers, Phys. Rev. B **95**, 245126 (2017).
[42] S. Vijay, J. Haah, and L. Fu, A new kind of topological quantum order: A dimensional hierarchy of quasiparticles built from stationary excitations, Phys. Rev. B **92**, 235136 (2015).
[43] S. Vijay, J. Haah, and L. Fu, Fracton topological order, generalized lattice gauge theory, and duality, Phys. Rev. B **94**, 235157 (2016).
[44] C. Chamon, Quantum Glassiness in Strongly Correlated Clean Systems: An Example of Topological Overprotection, Phys. Rev. Lett. **94**, 040402 (2005).
[45] M. A. Levin and X.-G. Wen, String-net condensation: A physical mechanism for topological phases, Phys. Rev. B **71**, 045110 (2005).
[46] Z.-C. Gu, M. Levin, B. Swingle, and X.-G. Wen, Tensor-product representations for string-net condensed states, Phys. Rev. B **79**, 085118 (2009).
[47] A. Yu. Kitaev, Fault-tolerant quantum computation by anyons, Ann. Phys. (NY) **303**, 2 (2003).
[48] Y. Hu, Y. Wan, and Y.-S. Wu, Twisted quantum double model of topological phases in two dimensions, Phys. Rev. B **87**, 125114 (2013).
[49] S. Beigi, P. W. Shor, and D. Whalen, The quantum double model with boundary: condensations and symmetries, Commun. Math. Phys. **306**, 663 (2011).
[50] I. Affleck, T. Kennedy, E. H. Lieb, and H. Tasaki, Rigorous Results on Valence-Bond Ground States in Antiferromagnets, Phys. Rev. Lett. **59**, 799 (1987).
[51] I. Affleck, T. Kennedy, E. H. Lieb, and H. Tasaki, Valence bond ground states in isotropic quantum antiferromagnets, in *Condensed Matter Physics and Exactly Soluble Models* (Springer, New York, 1988), pp. 253–304.
[52] X. Chen, Z.-X. Liu, and X.-G. Wen, Two-dimensional symmetry-protected topological orders and their protected gapless edge excitations, Phys. Rev. B **84**, 235141 (2011).
[53] M. Hein, W. Dür, J. Eisert, R. Raussendorf, M. Nest, and H.-J. Briegel, Entanglement in graph states and its applications, arXiv:quant-ph/0602096.
[54] M. Rossi, M. Huber, D. Bruß, and C. Macchiavello, Quantum hypergraph states, New J. Phys. **15**, 113022 (2013).
[55] J. Dehaene and B. De Moor, Clifford group, stabilizer states, and linear and quadratic operations over GF(2), Phys. Rev. A **68**, 042318 (2003).
[56] M. Van den Nest, J. Dehaene, and B. De Moor, Graphical description of the action of local Clifford transformations on graph states, Phys. Rev. A **69**, 022316 (2004).
[57] M. Grassl, A. Klappenecker, and M. Rotteler, Graphs, quadratic forms, and quantum codes, in Proceedings of the 2002 IEEE International Symposium on Information Theory (IEEE, New York, 2002), p. 45.
[58] This can be generalized to affine function: both equals to zero and 1 are allowed. The RBM representation of toric code uses the case of $k = 4$.
[59] See Appendix A for more details.
[60] D. Schlingemann, Stabilizer codes can be realized as graph codes, Quantum Inf. Comput. **2**, 307 (2002).
[61] V. Aggarwal and A. R. Calderbank, Boolean functions, projection operators, and quantum error correcting codes, IEEE Trans. Inf. Theory **54**, 1700 (2008).
[62] J.-Y. Cai, P. Lu, and M. Xia, The complexity of complex weighted Boolean #CSP, J. Comput. Syst. Sci. **80**, 217 (2014).
[63] J.-Y. Cai, H. Guo, and T. Williams, Clifford gates in the Holant framework, Theor. Comput. Sci. **745**, 163 (2018).
[64] E. Hostens, J. Dehaene, and B. De Moor, Stabilizer states and Clifford operations for systems of arbitrary dimensions and modular arithmetic, Phys. Rev. A **71**, 042315 (2005).
[65] S. Anders and H. J. Briegel, Fast simulation of stabilizer circuits using a graph-state representation, Phys. Rev. A **73**, 022334 (2006).
[66] A. Kitaev, Anyons in an exactly solved model and beyond, Ann. Phys. (NY) **321**, 2 (2006).
[67] O. Buerschaper, Twisted injectivity in projected entangled pair states and the classification of quantum phases, Ann. Phys. (NY) **351**, 447 (2014).
[68] R. Dijkgraaf and E. Witten, Topological gauge theories and group cohomology, Commun. Math. Phys. **129**, 393 (1990).
[69] M. de Wild Propitius, (Spontaneously broken) Abelian Chern-Simons theories, Nucl. Phys. B **489**, 297 (1997).
[70] For details, see Appendix B.
[71] B. Yoshida, Topological phases with generalized global symmetries, Phys. Rev. B **93**, 155131 (2016).
[72] M. Cheng, Z.-C. Gu, S. Jiang, and Y. Qi, Exactly solvable models for symmetry-enriched topological phases, Phys. Rev. B **96**, 115107 (2017).
[73] X. Chen, Symmetry fractionalization in two dimensional topological phases, Rev. Phys. **2**, 3 (2017).
[74] S. Aaronson and D. Gottesman, Improved simulation of stabilizer circuits, Phys. Rev. A **70**, 052328 (2004).
[75] Y.-H. Zhang, Z.-A. Jia, Y.-C. Wu, and G.-C. Guo, An efficient algorithmic way to construct Boltzmann machine representations for arbitrary stabilizer code, arXiv:1809.08631.